Sub-MHz spectral dip in a resonator-free twistedgain medium

Neel Choksi (neel.choksi@mail.utoronto.ca)
University of Toronto https://orcid.org/0000-0002-7583-8815
Yi Liu
University of Toronto
Rojina Ghasemi
University of Toronto
Li Qian
University of Toronto

Article

Keywords: Sub-MHz, brillouin gain, commercial spun fiber

Posted Date: June 17th, 2021

DOI: https://doi.org/10.21203/rs.3.rs-440353/v4

Sub-MHz spectral dip in a resonator-free twisted gain medium

NEEL CHOKSI[1*], YI LIU[1], ROJINA GHASEMI[1], LI QIAN [1*]

[1] *Department of Electrical and Computer Engineering, University of Toronto, 10 Kings College Road, Toronto, Ontario M5S 3G4, Canada*

[*] *neel.choksi@mail.utoronto.ca, l.qian@utoronto.ca*

Abstract: Ultra-narrow optical spectral features have broad applications in spectroscopy, slow light, and sensing. Features approaching sub-MHz, or equivalently, Q-factors approaching 1 billion and beyond, are challenging to obtain in solid-state systems, ultimately limited by loss. We present a new paradigm to achieve tunable sub-MHz spectral features at room temperature without resonators. We exploit gain-enhanced polarization pulling in a twisted birefringent medium where polarization eigenmodes are frequency-dependent. Using Brillouin gain in a commercial spun fiber, we experimentally achieve a 0.72 MHz spectral dip, the narrowest backward Brillouin scattering feature ever reported. Further optimization can potentially reduce the linewidth to <0.1 MHz. Our approach is simple and broadly applicable, offering on-demand tunability and high sensitivity, opening a new paradigm for microwave photonic filters, slow light, and optical sensing.

Introduction

Ultra-narrow resonances are highly sought-after for a wide range of applications such as slow-light [1,2] and information storage [3–5], high precision sensing [6], microwave photonics [7–10], spectroscopy [11], frequency stabilization [12], light detection and ranging (LIDAR) [13,14], and optical gyroscopes [15–17]. Narrowing the linewidth further to sub-MHz range (or equivalently, increasing the Q factors to approaching a billion and beyond) is very challenging, but highly desirable as it greatly improves the key performance metrics, across all applications [18]. For example, when a sub-MHz transparency is induced via Brillouin scattering in a high-Q silica resonator [3], it produced slow-light with a delay-bandwidth product 5 orders of magnitude higher than the next highest reported delay-bandwidth product in Brillouin based systems.

Such favourable performance improvements have stimulated phenomenal progress in obtaining narrow resonances through platforms such as gas-phase atomic systems [19, 20], photonic crystal cavities [12, 21–23], whispering gallery mode (WGM) [24, 25], and microring resonators [26–28], slow-light fiber Bragg gratings (FBGs) [2], and phase-shifted FBGs [29]. However, despite significant progress, there remain many challenges with these platforms.

While narrow spectral features can be realized in gas-phase atomic systems [19, 20], they typically require low temperatures and low pressure vacuums, making them bulky, expensive and impractical. Solid-state systems such as photonic crystal cavities [12, 21–23], WGM [24, 25] and microring resonators [26–28] are much more preferable, but they usually require complex and costly fabrication steps like chemical-mechanical polishing and high temperature annealing to obtain sub-MHz resonances [30]. Specialty FBGs, such as π-phase-shifted FBGs have also been shown to exhibit narrow resonances [29], but their linewidths are limited to a few MHz due to their intrinsic losses. Recently, efforts have been made to further narrow down the linewidth of a slow-light FBG [2] by using a gain medium to offset the intrinsic loss. But to achieve the narrowest resonance of 8.5 fm ($\sim$1.1 MHz), the FBGs need to be probed with very low signal powers ($<$ –50 dBm), limiting its practical use due to low signal-to-noise ratios.

Stimulated Brillouin scattering (SBS) is another technique to realize narrow spectral features. Both forward and backward SBS are possible, but forward SBS involves transverse acoustic modes and is far weaker in conventional single-mode waveguides than backward SBS [31]. Forward SBS in an ultrahigh-Q micro-resonator has demonstrated sub-MHz features [3, 4], but achieving and maintaining triple resonance (two optical and one acoustic resonances) in an ultrahigh Q resonator is no easy feat. Backward SBS, on the other hand, is easily obtainable in conventional waveguides, but its linewidth is a few tens of MHz in most solids [31, 32]. Recent efforts made to further narrow the SBS feature include making an optical analogue of electromagnetically induced absorption (EIA) [33], using Brillouin gain shaping [7], as well as combining SBS with an ultrahigh Q resonator [8], though only the latter [8] has achieved sub-MHz bandwidth. However, as with other SBS-resonator combination experiments, it requires precise alignment between the SBS peak and one of the resonances of the ultrahigh-Q resonator. Obtaining and maintaining such alignment over time can be a major challenge. Moreover, the configuration becomes significantly more complex with the added resonator.

In this work, we propose an entirely new paradigm to realize a sub-MHz, tunable spectral feature without using any resonator. We exploit gain-enhanced polarization pulling in a twisted

birefringent medium with frequency-dependent polarization eigenmodes. To demonstrate a specific realization, we use backward SBS in a commercial spun birefringent fiber (SBF) and experimentally achieve a 0.72 MHz spectral dip, which is to our knowledge, the narrowest backward SBS spectral feature ever reported. Furthermore, the configuration is extremely simple, no different from a conventional SBS arrangement, and no need for resonator alignment or stabilization, as it is resonator-free.

An SBF is an elliptically birefringent fiber, fabricated by spinning the birefringent preform while drawing the fiber, resulting in two *elliptically* polarized eigenmodes. Unlike conventional birefringent fibers (i.e., polarization-maintaining fibers or PMF), the elliptical eigenmodes of the SBF are dependent on both the twist (spun) period and the beat length of the SBF, and are therefore frequency-dependent [34]. When pump and signal are launched into the SBF in orthogonal polarization eigenmodes, for the pump and signal frequencies, respectively, they remain nearly orthogonal throughout the fiber, and therefore the signal experiences minimal gain. Any minute deviation in the signal frequency causes its eigenmode to deviate from its launch polarization, and due to the positive feedback of the Brillouin gain (polarization pulling effect), the signal polarization is pulled quickly toward the pump polarization, causing the signal field to experience a high Brillouin gain. The frequency-dependence of the eigenmode, together with the polarization pulling effect of the Brillouin gain, leads to a sub-MHz spectral dip in the Brillouin gain spectrum, which, as we will subsequently demonstrate, is tunable on-demand both in linewidth, depth, and frequency.

Theoretical Framework

An SBF is characterized by its twist rate ($k_t = \frac{2\pi}{L_t}$) and its unspun linear birefringence ($k_{bs/p} = \frac{2\pi}{L_b(\nu_{s/p})}$), where L_t and $L_b(\nu)$ are the twist period and the frequency-dependent beat length of the SBF, respectively, ν is the frequency of the electric field, and the subscripts s and p denote the signal and pump frequencies, respectively. We neglect the torsion induced birefringence, as SBF is twisted when it is in the molten state with negligible stress due to torsion.

Based on an SBS model for single-mode fiber (SMF) [35–37], we develop the SBS model in SBF with the configuration shown in Fig. 1. The signal field is launched into SBF at z = 0, while the pump is launched at z = L, where L is the length of SBF. The twist is modeled using a right-handed rotating frame of reference whose coordinates (ξ, η, z) are aligned with the fast and slow axes of the fiber locally. Hence, the (ξ, η, z) coordinates are rotating with z at the twist rate

k_t. The (x,y,z) coordinate system is considered to be the fixed frame of reference, and without the loss of generality, it is assumed that at z = 0, the fixed frame of reference is aligned with the rotating frame of reference.

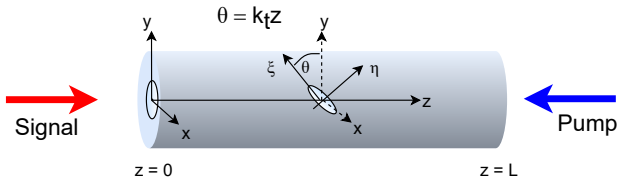

Fig. 1. The fixed coordinate system (x,y,z) and the right-handed rotating coordinate system (ξ,η,z) are used for modeling of the SBS in spun fiber. The (ξ,η,z) coordinates are aligned with the fast and slow axes of the fiber locally, and rotating with z at the twist rate k_t. At the signal launching end, i.e., $z = 0$, the fixed frame of reference is aligned with rotating frame of reference.

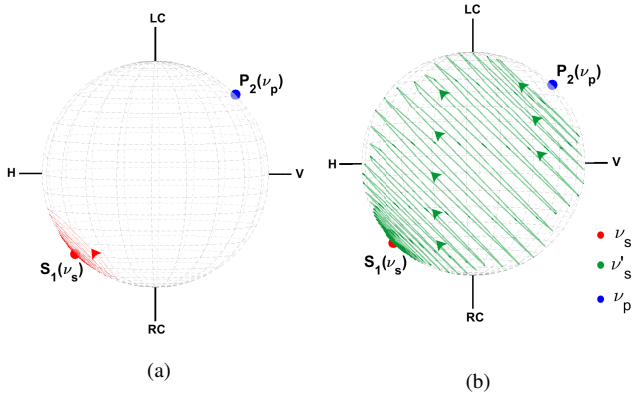

Fig. 2. Simulated signal polarization evolution (indicated by the red and green traces with arrows on a Poincaré sphere) along the SBF, for different signal frequencies: (a) $\nu_s = \nu_p - \Omega_o$ (b) $\nu_s' = \nu_s + 0.5$ MHz. For both (a) and (b), the pump launch polarization corresponds to the eigenmode $\mathbf{P}_2(\nu_p)$, and the signal launch polarization corresponds to $\mathbf{S}_1(\nu_s)$, which is an eigenmode for ν_s, but not an eigenmode for the signal frequency of ν_s'. Therefore, the signal polarization for case (a) is maintained, and the signal remains nearly orthogonal throughout the fiber. In contrast, the signal polarization for case (b) is not maintained in the SBF, rather, it is pulled towards $\mathbf{P}_2(\nu_p)$. On the Poincaré sphere, H denotes horizontal polarization, V denotes vertical polarization, LC denotes left-circular polarization, and RC denotes right-circular polarization.

In the (ξ,η,z) coordinate system, the non-normalized Jones vector for the signal field

propagating in +z direction at a position z is denoted by $\vec{A}_{rs}(z)$, and for the pump field, propagating in -z direction, it is denoted by $\vec{A}_{rp}(z)$. The amplitudes of $\vec{A}_r(z)$ are chosen such that their squared values correspond to the optical powers in the mode. In the (x,y,z) coordinate system, the non-normalized Jones vectors for the signal and the pump fields are denoted by $\vec{A}_s(z)$ and $\vec{A}_p(z)$, respectively. The Jones vectors in these two coordinate systems are related by a rotation matrix $\boldsymbol{R}(k_t z)$.

$$\vec{A}_{rs/p}(z) = \boldsymbol{R}(k_t z)\vec{A}_{s/p}(z) \tag{1}$$

The signal frequency (ν_s) is downshifted from the pump frequency (ν_p) by a frequency Ω (ν_s=$\nu_p - \Omega$). Using Eq. (1), the coupled differential equations governing the polarization evolution of signal and pump fields in the (x,y,z) coordinate system [37] are converted to the (ξ, η, z) coordinate system. In Eqs. (2) and (3), the first term represents the polarization rotation in SBF without gain, and the second term represents the SBS term.

$$\frac{d\vec{A}_{rs}(z)}{dz} = \frac{d\boldsymbol{T}_s(z)}{dz}\boldsymbol{T}_s^{\dagger}(z)\vec{A}_{rs}(z) + \gamma(\Omega, \Omega_0)(\vec{A}_{rp})\Big((\vec{A}_{rp})^{\dagger}(z)\vec{A}_{rs}(z)\Big) \tag{2}$$

$$\frac{d\vec{A}_{rp}(z)}{dz} = \frac{d\boldsymbol{T}_p(z)}{dz}\boldsymbol{T}_p^{\dagger}(z)\vec{A}_{rp}(z) + \gamma(\Omega, \Omega_0)(\vec{A}_{rs})\Big((\vec{A}_{rs})^{\dagger}(z)\vec{A}_{rp}(z)\Big) \tag{3}$$

Here, $\gamma(\Omega, \Omega_0)$ [W m]$^{-1}$ is the Brillouin gain coefficient, which is modelled by a Lorentzian function, where Ω_0 is the central Brillouin frequency shift. $\boldsymbol{T}_{s/p}$ [38–40] is the transfer matrix for the signal (subscript s) and the pump (subscript p) field, and it is given by :

$$\boldsymbol{T}_{s/p}(z) = \begin{bmatrix} cos(k_{bts/p}z) - j\frac{k_{bs/p}}{k_{bts/p}}sin(k_{bts/p}z) & -\frac{k_t}{k_{bts/p}}sin(k_{bts/p}z) \\ \frac{k_t}{k_{bts/p}}sin(k_{bts/p}z) & cos(k_{bts/p}z) + j\frac{k_{bs/p}}{k_{bts/p}}sin(k_{bts/p}z) \end{bmatrix}, \tag{4}$$

where $k_{bts/p} = \sqrt{k_{bs/p}^2 + k_t^2}$. The eigenmodes of the transfer matrix $\boldsymbol{T}_{s/p}(z)$ are denoted by $\boldsymbol{S_1}$ ($\boldsymbol{P_1}$) and $\boldsymbol{S_2}$ ($\boldsymbol{P_2}$) at the signal (pump) frequency, which are given by:

$$\boldsymbol{S}_1 = \frac{1}{m_s}\begin{bmatrix} i\left(\frac{k_{bs}+k_{bts}}{k_t}\right) \\ 1 \end{bmatrix},\ \boldsymbol{S}_2 = \frac{1}{m_s'}\begin{bmatrix} i\left(\frac{k_{bs}-k_{bts}}{k_t}\right) \\ 1 \end{bmatrix}$$

$$\boldsymbol{P}_1 = \frac{1}{m_p}\begin{bmatrix} i\left(\frac{k_{bp}+k_{btp}}{k_t}\right) \\ 1 \end{bmatrix},\ \boldsymbol{P}_2 = \frac{1}{m_p'}\begin{bmatrix} i\left(\frac{k_{bp}-k_{btp}}{k_t}\right) \\ 1 \end{bmatrix},$$

where $m_{s/p}$ and $m'_{s/p}$are the normalizing factors.

As can be verified, the eigenmodes $\boldsymbol{S}_1$ and $\boldsymbol{P}_2$, and $\boldsymbol{P}_1$ and $\boldsymbol{S}_2$ are nearly orthogonal. (Refer to the blue and red dots on the Poincaré sphere in Fig. 2a). Here we use “nearly" because the pump and signal frequencies are different slightly, and therefore the eigenmode for the pump is not exactly orthogonal to the eigenmode for the signal. Nevertheless, these eigenmodes are well maintained throughout their propagation in the SBF [41], even in the presence of Brillouin gain. As a result, the signal and pump are nearly orthogonal throughout the fiber if they are launched into these eigenmodes. (Refer to the red trace on the Poincaré sphere in Fig. 2a for the signal polarization evolution along the fiber). It is important to note here that the signal eigenmode is a function of its frequency. Changing its frequency without changing its launch polarization will result in launching into a non-eigenmode.

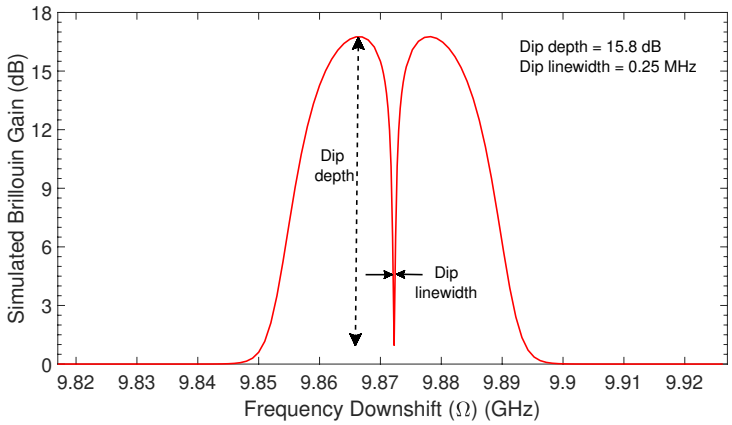

Fig. 3. Simulation result demonstrating a sub-MHz spectral dip in backward Brillouin gain spectrum of SBF. The input signal polarization is the same for all signal frequencies, and it corresponds to the eigenmode $\boldsymbol{S_1}$ at the dip frequency (9.8723 GHz). At any other frequency, the launched signal polarization deviates from the eigenmode for that frequency. The input pump polarization is $\boldsymbol{P_2}$. The linewidth of the dip is 0.25 MHz when measured at 3 dB from the minimum. The simulation parameters are: L = 900 m, L_t = 3 mm, $L_b(\nu_p)$ = 26 mm, input pump power = 16.9 dBm, input signal power = -12 dBm, and pump wavelength = 1554.616 nm.

The signal field experiences minimum Brillouin gain when the signal and pump fields are launched as orthogonal polarization eigenmodes ($\mathbf{S}_1(\nu_s)$ and $\mathbf{P}_2(\nu_p)$) of the SBF, and they remain nearly orthogonal along the length of SBF (Fig. 2a). With a minute change in signal frequency from ν_s to ν_s', the signal launch polarization ($\mathbf{S}_1(\nu_s)$) is no longer an eigenmode for ν_s', and the signal polarization will no longer remain orthogonal to the pump polarization due to

the polarization pulling effect [37], as shown in Fig. 2b. As a result, the signal at ν_s' experiences a much higher Brillouin gain. Thus, this frequency dependence of the eigenmodes along with the Brillouin gain leads to a narrow spectral dip in the Brillouin gain spectrum. The simulation result is shown in Fig. 3. A spectral dip with a linewidth of 0.25 MHz (measured at 3 dB from the minimum) is clearly observed.

It is important to emphasize that this dip is present only in moderately spun birefringent fibers. More specifically, it only occurs when the eigenmodes are elliptical. (Fig. 2 illustrates an example, where $\boldsymbol{S_1}$ and $\boldsymbol{P_2}$ are half-way between circular and linear polarization.) As shown in Fig. 5, the dip disappears either when linear birefringence dominates (e.g., in PMF) or when circular birefringence dominates (e.g, when twist rate is very high). In both cases, the eigenmodes become insensitive to frequency. Interestingly, this dip is also not observed in SMF (see Fig. 4), when both beat length and twist period become large. Therefore this spectral dip has been elusive, and was never observed in SMF or PMF. This work is the first time such a spectral dip is ever analyzed and observed.

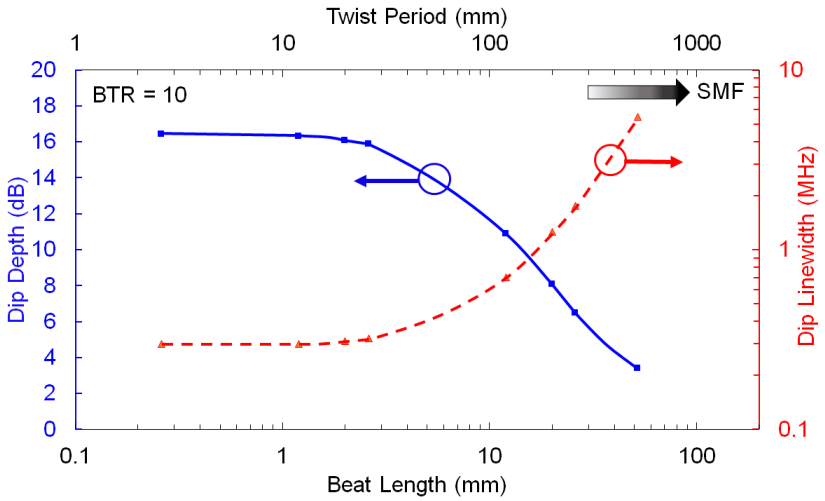

Fig. 4. Simulation result showing the depth (maximum - minimum gain) and the linewidth (measured at 3 dB from minimum gain) of the spectral dip as a function of $L_b(\nu_p)$ and L_t when the birefringence to twist ratio (BTR) is fixed at 10. The simulation parameters are: L = 900 m, input signal power = -12 dBm, and input pump power = 16.9 dBm. The symbols are simulation data points, and the lines are guides to the eye.

To gain more insights into the behaviour of this spectral dip and how it is affected by linear

birefringence and twist rate, let us define a Birefringence-to-Twist Ratio (BTR = k_{bp}/k_t = $L_t/L_b(\nu_p)$). We first analyze the dip depth and linewidth as a function of a fixed BTR of 10, meaning that the unspun linear birefringence is 10 times the twist period. As seen in Fig. 4, for BTR = 10, the dip disappears if the beat length (and twist period) becomes too large. In the extreme, the spun fiber becomes an SMF. In the opposite direction, when the beat length (and twist period) decreases, the dip sharpens and deepens, until the dip depth and linewidth converge to limiting values. In other words, for a fixed BTR, when the beat length (and twist period) is sufficiently small, the dip reaches its sharpest limit and no longer narrows or deepens. This is useful for practical considerations. It means that one does not need to fabricate SBFs with impractically high birefringence or twist rate to achieve the narrowest dip. A beat length and twist period of a few mm is practically achievable.

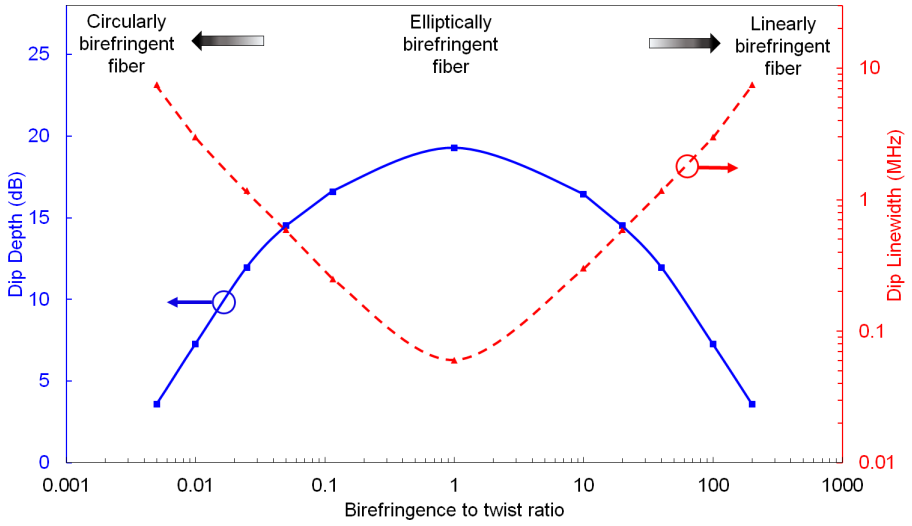

Fig. 5. Simulation result showing the depth (maximum - minimum gain) and the linewidth (measured at 3 dB from minimum gain) of the narrowest spectral dip realized at a given birefringence to twist ratio (BTR) of SBF. For all the ratios, the beat length of SBF is kept at 0.26 mm. Other parameters used in the simulation are: L = 900 m, input signal power = -12 dBm, and input pump power = 16.9 dBm. The symbols are simulation data points, and the lines are guides to the eye.

Next, we analyze the dip behaviour as a function of BTR (Fig. 5), keeping the beat length sufficiently small (L_b = 0.26 mm). At very low BTRs (e.g., < 10^{-3}), the SBF behaves like a circularly birefringent fiber, and for high BTRs (e.g., > 10^3), the SBF behaves like a linearly birefringent fiber (such as the PMF). At both extremes, the dip disappears, and the dip width is

so wide that essentially there is no notable dip. On the other hand, when BTR lies in the range of [0.05, 20], the dip linewidth is <1 MHz, and the depth is high (>10 dB). Predictably, the dip is narrowest (with a linewidth of 0.06 MHz) and deepest (with a depth of 19 dB) at BTR = 1. This dip linewidth is equivalent to a Q-factor greater than 3 billion if a resonator was used.

The spectral location of this dip can be tuned in real-time (on demand) by changing either the pump wavelength or the input polarization, the latter is indicated in Fig. 6. The spectral linewidth of the dip can be tuned by varying the pump power, and it is shown in Fig. 7.

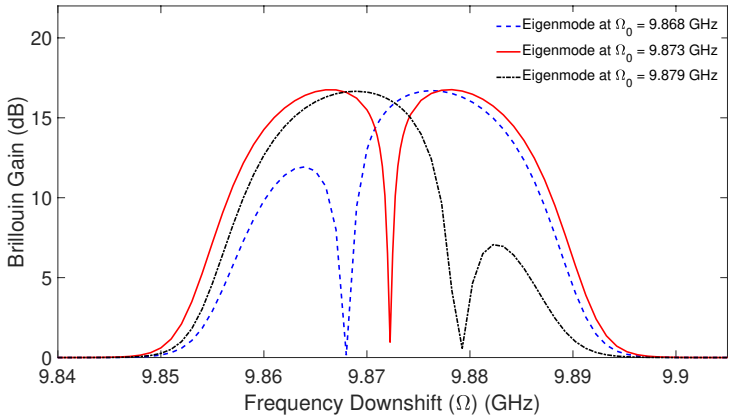

Fig. 6. Simulation result showing the tunability of the spectral position of the dip by varying the input signal polarization, while keeping the pump polarization fixed. Input signal polarizations are the eigenmodes of SBF calculated at different Brillouin frequency shifts (Ω_0) from the pump. The simulation parameters are: L = 900 m, L_t = 3 mm, $L_b(\nu_p)$ = 26 mm, input pump power = 16.9 dBm, and input signal power = -12 dBm.

With our approach, by controlling the pump frequency, pump power and signal polarization, one has sufficient degrees of freedom to tune the dip frequency, linewidth, and depth, in real-time. This has an important practical significance in microwave photonics.

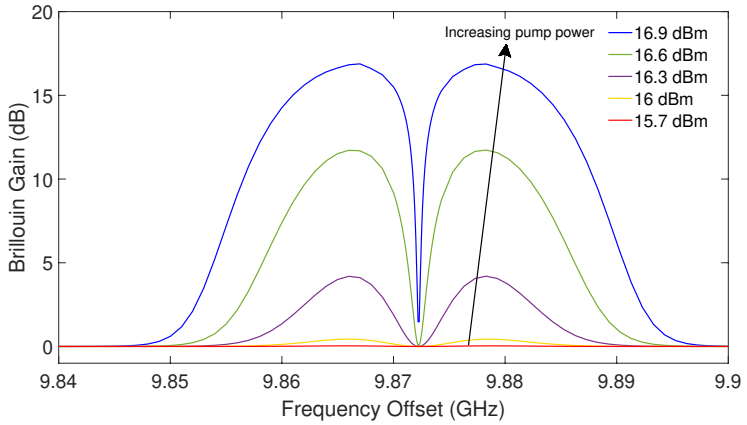

Fig. 7. Simulation result showing the tunability of the spectral linewidth of the dip in the Brillouin gain spectrum of SBF by varying the pump power. Input signal polarization is the eigenmode of SBF calculated at a frequency downshift of 9.8723 GHz. The simulation parameters are: L = 900 m, L_t = 3 mm, $L_b(\nu_p)$ = 26 mm, and input signal power = -12 dBm.

Experimental Results

For an experimental demonstration, we use a commercial SBF manufactured by IVG Fiber [42]. The beat length and the twist period of this fiber is 26 mm and 3 mm, respectively. Note that this fiber does not have the optimal BTR of 1, but it is the only SBF available to us. The experimental arrangement shown in Fig. 8 is used to obtain the Brillouin gain spectrum of SBF. In the first arm, the pump field is amplified, and its polarization is adjusted before launching into SBF using a polarization controller. In the second arm, the signal field is amplified, and amplitude-modulated to produce two sidebands. The lower frequency sideband is selected by a tunable filter (AOS ultra-narrow filter with 0.12 nm passband bandwidth). The signal polarization is adjusted before launching into SBF, and its frequency is swept over the Brillouin gain range by sweeping the RF driving frequency of the electro-optic modulator (EOM).

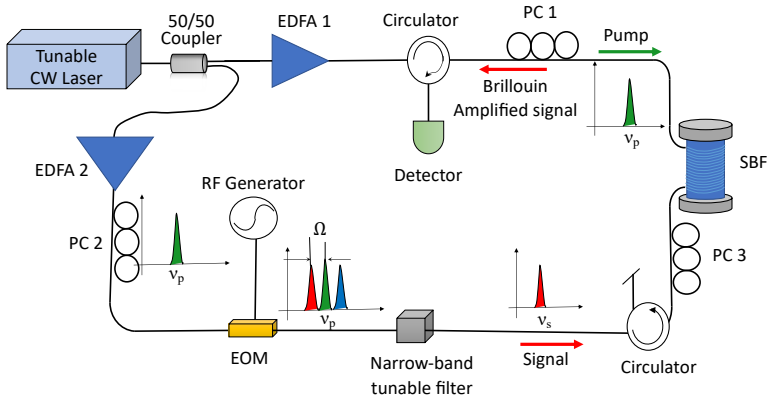

Fig. 8. Experimental set up to measure Brillouin gain: Pump and signal are generated from the same CW laser source. Signal frequency is downshifted from the pump by selecting the lower frequency sideband (red) of the modulated signal after the electro-optic modulator (EOM). Pump and signal polarizations are controlled by the polarization controllers PC1 and PC3, respectively.

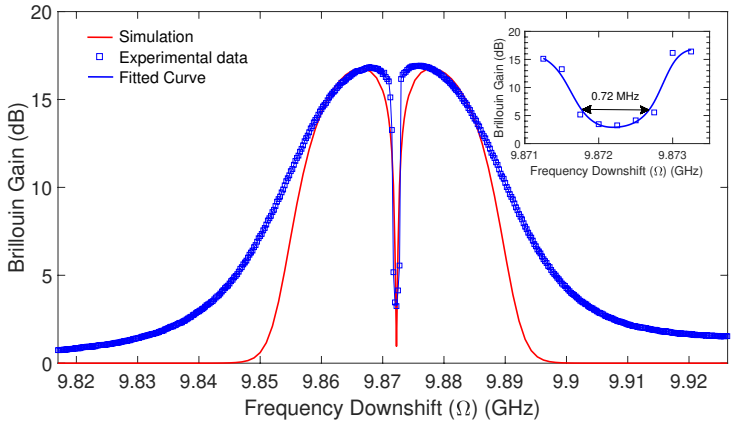

Fig. 9. Comparison of the Brillouin gain spectrum obtained via simulation and experiment. For the simulation, signal and pump fields are launched as orthogonal polarization eigenmodes $\boldsymbol{S_1}$ and $\boldsymbol{P_2}$ into the SBF, for a particular pump frequency (ν_p) and the corresponding downshifted signal frequency ($\nu_s = \nu_p - \Omega$), in counter-propagating directions. The parameters used for the simulation are similar to the experimental parameters, and they are as following: L = 900 m, L_t = 3 mm, $L_b(\nu_p)$ = 26 mm, input pump power = 16.9 dBm, and input signal power = -12 dBm.

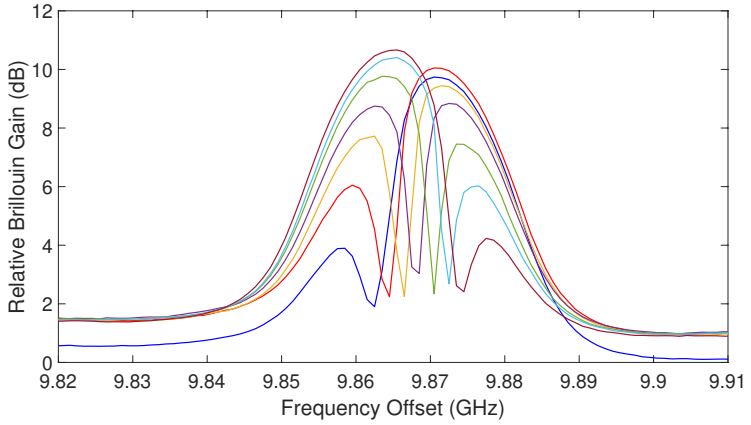

Fig. 10. Experimental result showing the tunability of the spectral position of the dip in the Brillouin gain spectrum of SBF by varying the input signal polarization, while keeping the pump polarization fixed. The experimental parameters are: L = 900 m, L_t = 3 mm, $L_b(\nu_p)$ = 26 mm, input pump power = 16.9 dBm, and input signal power = -12 dBm.

The experimental and the simulation results are compared in Fig. 9, and good agreement between the two is evident. The simulated dip linewidth is 0.25 MHz, whereas the experimental dip linewidth is 0.72 MHz, obtained from the least squares polynomial fit of the experimental data near the dip (see inset of Fig. 9). The experimental dip being wider than the simulation dip is likely due to the fact that a lower spectral resolution is used in the measurement (0.25 MHz) than in the simulation (0.01 MHz). Given the experimental dip is actually narrower than the simulation dip in the high gain region, we expect that higher spectral resolution may result in a narrower dip more consistent with the simulation results. The experimental gain shape on the wings of the Brillouin gain deviates from the simulation shape, likely due to the fact that the experimental lineshape is not strictly a Lorentzian lineshape, as is used for the simulation. The tunability of the spectral location of this dip by changing the input polarization is experimentally verified, and the result is presented in Fig. 10.

Discussion

As we have seen, both theoretically and experimentally, the sub-MHz spectral dip is a result of polarization pulling in an elliptically birefringent medium. The filtering effect in a birefringent medium is reminiscent of birefringent filters, of which Lyot filter ([43] and Šolc [43, 44] filter

are two well-known examples. The SBF is analogues to a fan-Šolc filter [43, 44] except for three facts: (a) the birefringence axis is continuously rotating in SBF, whereas in a fan-Šolc filter, discrete birefringent plates have discrete rotation angles; (b) the overall rotation angle in SBF is not limited to $\pi/2$, and in fact is many orders of magnitude larger; (c) there are no polarizers in SBF as in the Šolc filter. It is this last point that warrants further discussion. In our demonstration, instead of polarizers (which in essence introduce polarization-dependent loss), we have Brillouin gain, which introduces polarization-dependent gain. This is a crucial distinction, and is the reason why we can achieve such a narrow spectral feature. Had we replaced the Brillouin gain with a pair of polarizers, and even if we meet the Šolc filter conditions, we would not have obtained sharp spectral features. In fact, it can be shown that, with the same length of the fiber (that is, the same amount of polarization rotation), if polarizers are used (either at the two ends of the fiber or distributed periodically throughout the fiber length), the resulting Šolc filter feature is on the order of tens of GHz. So, why are we able to obtain sub-MHz features when we use polarization-dependent gain? The answer lies in the positive feedback the gain produces. Much like the linewidth narrowing when gain builds up in a lasing process, the dip becomes narrower and narrower when gain increases (see Fig. 7), resulting in a 5 orders of magnitude narrowing of the passive filter feature.

Therefore, in a nutshell, the innovation of our method lies in the mechanism of enhancing birefringent filtering using a polarization-dependent gain to create a positive feedback. It is to our knowledge the first proposal and demonstration of such a mechanism, which can be broadly implemented using other birefringent media and gain mechanisms, and therefore can potentially lead to a paradigm shift in the pursuit of ultra-narrow spectral features.

Conclusion

In conclusion, we have demonstrated a resonator-free approach of generating a sub-MHz tunable spectral dip at room-temperature by exploiting polarization pulling in a medium with frequency-dependent polarization eigenmodes. As a specific realization, we have experimentally demonstrated a 0.72 MHz spectral dip in the Brillouin gain spectrum of a commercial spun fiber. The observed dip linewidth of 0.72 MHz is equivalent to a Q factor of 267 million if a resonator were used. The linewidth, depth and the location of the dip can be tuned on demand by controlling the pump frequency, the pump power, and the input polarization of the signal. Moreover, with an optimal spun birefringent fiber, the dip linewidth is predicted to be as low as

≤ 0.1 MHz, corresponding to a Q factor of 2 billion.

Even though the current analysis of this spectral dip is carried out in fiber, this ultra-narrow feature can potentially be realized in integrated waveguides, using, for instance, chiral birefringent material or a helical waveguide. The gain mechanism is also not limited to SBS. With a broadband polarization-dependent gain (e.g., Raman gain, parametric gain), one might be able to realize a comb of narrow spectral dips. The essential elements required to realize such narrow spectral dips are a polarization-dependent gain and a rotating birefringence with frequency-dependent polarization eigenmodes.

The simplicity in the implementation of this technique, as well as the ultra-narrow spectral feature and the easily attainable tunability of the dip, may open a wide range of potential applications, such as ultrahigh resolution optical sensing, ultra-narrow band tunable optical filters for microwave photonics, slow-light and information storage applications.

Data Availability

The data that support the findings of this study are available from the corresponding authors upon reasonable request.

Code Availability

All code and simulation data files used to obtain the described simulation results results are available from the corresponding authors upon reasonable request.

References

1. K. L. Tsakmakidis, O. Hess, R. W. Boyd, and X. Zhang, "Ultraslow waves on the nanoscale," Science **358** (2017).
2. P.-B. Vigneron, T. Boilard, E. Balliu, A. L. Broome, M. Bernier, and M. J. Digonnet, "Loss-compensated slow-light fiber bragg grating with 22-km/s group velocity," Opt. Lett. **45**, 3179–3182 (2020).
3. J. Kim, M. C. Kuzyk, K. Han, H. Wang, and G. Bahl, "Non-reciprocal brillouin scattering induced transparency," Nat. Phys. **11**, 275–280 (2015).
4. C.-H. Dong, Z. Shen, C.-L. Zou, Y.-L. Zhang, W. Fu, and G.-C. Guo, "Brillouin-scattering-induced transparency and non-reciprocal light storage," Nat. communications **6**, 1–6 (2015).
5. C. Wang, X. Jiang, G. Zhao, M. Zhang, C. W. Hsu, B. Peng, A. D. Stone, L. Jiang, and L. Yang, "Electromagnetically induced transparency at a chiral exceptional point," Nat. Phys. **16**, 334–340 (2020).

6. A. Arora, M. Esmaeelpour, M. Bernier, and M. J. Digonnet, "High-resolution slow-light fiber bragg grating temperature sensor with phase-sensitive detection," Opt. letters **43**, 3337–3340 (2018).
7. A. Choudhary, Y. Liu, B. Morrison, K. Vu, D.-Y. Choi, P. Ma, S. Madden, D. Marpaung, and B. J. Eggleton, "High-resolution, on-chip rf photonic signal processor using brillouin gain shaping and rf interference," Sci. reports **7**, 1–9 (2017).
8. H. S. Wen, M. Li, W. Li, and N. H. Zhu, "Ultrahigh-q and tunable single-passband microwave photonic filter based on stimulated brillouin scattering and a fiber ring resonator," Opt. letters **43**, 4659–4662 (2018).
9. Y. Liu, A. Choudhary, D. Marpaung, and B. J. Eggleton, "Integrated microwave photonic filters," Adv. Opt. Photonics **12**, 485–555 (2020).
10. D. Marpaung, J. Yao, and J. Capmany, "Integrated microwave photonics," Nat. photonics **13**, 80–90 (2019).
11. M.-G. Suh, Q.-F. Yang, K. Y. Yang, X. Yi, and K. J. Vahala, "Microresonator soliton dual-comb spectroscopy," Science **354**, 600–603 (2016).
12. M. Anderson, N. Pavlov, J. Jost, G. Lihachev, J. Liu, T. Morais, M. Zervas, M. Gorodetsky, and T. Kippenberg, "Highly efficient coupling of crystalline microresonators to integrated photonic waveguides," Opt. letters **43**, 2106–2109 (2018).
13. M.-G. Suh and K. J. Vahala, "Soliton microcomb range measurement," Science **359**, 884–887 (2018).
14. P. Trocha, M. Karpov, D. Ganin, M. H. Pfeiffer, A. Kordts, S. Wolf, J. Krockenberger, P. Marin-Palomo, C. Weimann, S. Randel *et al.*, "Ultrafast optical ranging using microresonator soliton frequency combs," Science **359**, 887–891 (2018).
15. J. Li, M.-G. Suh, and K. Vahala, "Microresonator brillouin gyroscope," Optica **4**, 346–348 (2017).
16. W. Liang, V. S. Ilchenko, A. A. Savchenkov, E. Dale, D. Eliyahu, A. B. Matsko, and L. Maleki, "Resonant microphotonic gyroscope," Optica **4**, 114–117 (2017).
17. Y.-H. Lai, M.-G. Suh, Y.-K. Lu, B. Shen, Q.-F. Yang, H. Wang, J. Li, S. H. Lee, K. Y. Yang, and K. Vahala, "Earth rotation measured by a chip-scale ring laser gyroscope," Nat. Photonics **14**, 345–349 (2020).
18. K. J. Vahala, "Optical microcavities," Nature **424**, 839–846 (2003).
19. C. Sayrin, C. Clausen, B. Albrecht, P. Schneeweiss, and A. Rauschenbeutel, "Storage of fiber-guided light in a nanofiber-trapped ensemble of cold atoms," Optica **2**, 353–356 (2015).
20. B. Gouraud, D. Maxein, A. Nicolas, O. Morin, and J. Laurat, "Demonstration of a memory for tightly guided light in an optical nanofiber," Phys. review letters **114**, 180503 (2015).
21. A. A. Savchenkov, V. S. Ilchenko, A. B. Matsko, and L. Maleki, "Kilohertz optical resonances in dielectric crystal cavities," Phys. Rev. A **70**, 051804 (2004).
22. I. S. Grudinin, V. S. Ilchenko, and L. Maleki, "Ultrahigh optical q factors of crystalline resonators in the linear regime," Phys. Rev. A **74**, 063806 (2006).
23. G. Liu, V. S. Ilchenko, T. Su, Y.-C. Ling, S. Feng, K. Shang, Y. Zhang, W. Liang, A. A. Savchenkov, A. B. Matsko *et al.*, "Low-loss prism-waveguide optical coupling for ultrahigh-q low-index monolithic resonators," Optica **5**, 219–226 (2018).
24. A. Shitikov, I. Bilenko, N. Kondratiev, V. Lobanov, A. Markosyan, and M. Gorodetsky, "Billion q-factor in silicon wgm resonators," Optica **5**, 1525–1528 (2018).
25. L. Wu, H. Wang, Q. Yang, Q.-x. Ji, B. Shen, C. Bao, M. Gao, and K. Vahala, "Greater than one billion q factor for on-chip microresonators," Opt. Lett. **45**, 5129–5131 (2020).
26. X. Ji, F. A. Barbosa, S. P. Roberts, A. Dutt, J. Cardenas, Y. Okawachi, A. Bryant, A. L. Gaeta, and M. Lipson, "Ultra-low-loss on-chip resonators with sub-milliwatt parametric oscillation threshold," Optica **4**, 619–624 (2017).

27. K. Y. Yang, D. Y. Oh, S. H. Lee, Q.-F. Yang, X. Yi, B. Shen, H. Wang, and K. Vahala, "Bridging ultrahigh-q devices and photonic circuits," Nat. Photonics **12**, 297–302 (2018).
28. M. W. Puckett, K. Liu, N. Chauhan, Q. Zhao, N. Jin, H. Cheng, J. Wu, R. O. Behunin, P. T. Rakich, K. D. Nelson *et al.*, "422 million intrinsic quality factor planar integrated all-waveguide resonator with sub-mhz linewidth," Nat. communications **12**, 1–8 (2021).
29. M. Jing, B. Yu, J. Hu, H. Hou, G. Zhang, L. Xiao, and S. Jia, "Impedance self-matching ultra-narrow linewidth fiber resonator by use of a tunable π-phase-shifted fbg," Sci. reports **7**, 1–11 (2017).
30. L. Chang, W. Xie, H. Shu, Q.-F. Yang, B. Shen, A. Boes, J. D. Peters, W. Jin, C. Xiang, S. Liu *et al.*, "Ultra-efficient frequency comb generation in algaas-on-insulator microresonators," Nat. communications **11**, 1–8 (2020).
31. A. Kobyakov, M. Sauer, and D. Chowdhury, "Stimulated brillouin scattering in optical fibers," Adv. optics photonics **2**, 1–59 (2010).
32. B. J. Eggleton, C. G. Poulton, P. T. Rakich, M. J. Steel, and G. Bahl, "Brillouin integrated photonics," Nat. Photonics **13**, 664–677 (2019).
33. A. B. Yelikar, R. Pant *et al.*, "Analogue of electromagnetically induced absorption in the microwave domain using stimulated brillouin scattering," Commun. Phys. **3**, 1–11 (2020).
34. E. Zhu, L. Qian, L. Helt, M. Liscidini, J. Sipe, C. Corbari, A. Canagasabey, M. Ibsen, and P. Kazansky, "Phase-matching with a twist: Second-harmonic generation in birefringent periodically poled fibers," JOSA B **27**, 2410–2415 (2010).
35. R. Stolen, "Polarization effects in fiber raman and brillouin lasers," IEEE J. Quantum Electron. **15**, 1157–1160 (1979).
36. R. W. Boyd, *Nonlinear optics* (Academic press, 2019).
37. A. Zadok, E. Zilka, A. Eyal, L. Thévenaz, and M. Tur, "Vector analysis of stimulated brillouin scattering amplification in standard single-mode fibers," Opt. express **16**, 21692–21707 (2008).
38. P. McIntyre and A. W. Snyder, "Light propagation in twisted anisotropic media: Application to photoreceptors," JOSA **68**, 149–157 (1978).
39. J.-i. Sakai and T. Kimura, "Birefringence and polarization characteristics of single-mode optical fibers under elastic deformations," IEEE J. Quantum Electron. **17**, 1041–1051 (1981).
40. H. Huang, *Microwave Approach to Highly-irregular Fiber Optics* (Wiley, 1998).
41. A. Yariv and P. Yeh, *Photonics: optical electronics in modern communications (the oxford series in electrical and computer engineering)* (Oxford University Press, Inc., 2006).
42. *The SBF is drawn from a rotating glass preform, IVG Fiber model LB1300.*
43. J. W. Evans, "The birefringent filter," JOSA **39**, 229–242 (1949).
44. I. Šolc, "Birefringent chain filters," JOSA **55**, 621–625 (1965).